Raman Tilt Prediction for Digital Twin Modelling of ROADM-based Transmission Systems

Rishu Raj*, Shuang Xie*, Zehao Wang#, Tingjun Chen#, and Daniel Kilper*
*CONNECT Centre, Trinity College Dublin, Ireland; #Duke University, Durham, NC, USA.

2024 IEEE Future Networks World Forum (FNWF) | 979-8-3503-7949-5/24/$31.00 ©2024 IEEE | DOI: 10.1109/FNWF63303.2024.11028801

Abstract — **Fulfilling the anticipated demands of future network technologies entails a plethora of challenges. Traditional approaches to tackle these challenges struggle with scalability in disaggregated systems, leading to a shift towards data-driven methods, especially machine learning (ML). Digital twins offer a cost-effective way to optimize network management and support decision-making. However, accurately predicting physical phenomena like stimulated Raman scattering (SRS) remains a challenge, as conventional physics-based models may fail due to variations in transmission spans. In this paper, we develop a deep neural network (DNN) model to predict the SRS-induced Raman tilt in optical fibers. The DNN is trained with data obtained from experiments on the COSMOS testbed, and its performance is benchmarked against established analytical models. Our results demonstrate that the proposed DNN has a mean absolute error between 0.03 dB – 0.12 dB.**

Keywords—digital twins, Raman tilt, DNN, future networks.

I. Introduction

Future network technologies like 6G have unprecedented needs for high bandwidth and low latency. These requirements can be largely met by advanced optical communication systems stretching from the network edge to the core [1]. The components of such networks must meet a variety of performance and control challenges with complexities arising from various factors, including non-linear impairments, component irregularities, and optical power dynamics that are influenced by wavelength and polarization-dependent effects in amplifiers and fiber spans [2]. Traditionally, these challenges have been managed through laboratory measurements, but with the adoption of disaggregated systems, these traditional approaches become inadequate and difficult to scale, as no single vendor oversees or tests the entire system end-to-end. Consequently, there is increasing interest in data collection and data-driven methods, particularly those involving machine learning (ML) [3], which are essential for advancing low-margin engineering and managing the aggravated control complexities in fully disaggregated systems [4]. To address these challenges, it is crucial to develop experimental platforms that can investigate the interactions between new control and management systems and the physical transmission effects they encounter.

Historically, optical networking experiments were conducted with a small number of nodes over relatively short distances such as a single transmission span. However, modern optical networks have expanded dramatically, enabling signal transmission across very long distances [5]. As the scale and cost of such experiments have grown, there is a pressing need for new methods to study physical effects on a larger scale and to understand how these effects interact with novel software controls, ML algorithms, and control hardware innovations. The shift towards data-driven controls for improved management and automation has also highlighted the need for new experimental emulation techniques, such as digital twins.

A digital twin is a virtual replica of a communication network that accurately replicates the devices, communication links, operating conditions, and applications found in the actual network [6]. By simulating various settings within a controlled environment and running multiple scenarios, digital twins provide a cost-effective way to evaluate performance, forecast the impact of network changes, optimize network management, and support decision-making processes [7]. However, digital twins require extensive datasets that accurately reflect the system's characteristics and performance under a wide range of operating conditions [8]. One method for gathering data involves using lab-based testbeds to collect datasets on individual components and then developing models that can be applied to the full system in the field. For example, inference on a deep neural network (DNN) trained on component data has already been applied to neural network models of optical amplifiers, predicting end-to-end signal power dynamics [9, 10]. Evidently, a critical decision in digital twin modelling is to choose between physics-based analytical models or data-driven ML models or a mixture of both. The physics of optical transmission is well understood, and physics-based models have been reliably used to manage and control optical systems.

Stimulated Raman scattering (SRS) is a well-known physical phenomenon in optical transmission systems, where optical power from shorter wavelength signals is transferred to longer wavelength signals via the fiber Raman interaction, creating a tilted spectrum at the fiber output. Recent studies have examined the effects of SRS in multi-band transmission [11]. In earlier studies, the effects of SRS could be accurately predicted for uniformly distributed wavelength division multiplexed (WDM) channels using a straightforward analytical formula based on a few basic assumptions [12 – 14]. However, variations in a transmission span—due to factors like splices and other defects—can cause significant deviations from these assumptions, particularly when WDM channels are not uniformly distributed, and channel powers vary because of wavelength-dependent power dynamics or engineering rules for different modulation formats. These factors can lead to considerable inaccuracies in predictions made by analytical models. ML-based models offer an alternative approach, but their ability to accurately predict SRS in WDM transmission systems has not been fully explored. In [15], the use of ML models for SRS prediction in variable channel configurations has been proposed and compared against the simplified analytical model of [13].

In this paper, we develop a DNN to predict the Raman tilt in optical fibres deployed in communication networks. It extends the work in [15] by simplifying the DNN model and improving its prediction performance. Moreover, we provide a more detailed analysis of different analytical models for the prediction of Raman tilt. For training and testing the proposed DNN-based prediction model, we collect data from WDM signals with various channel configurations in the open-

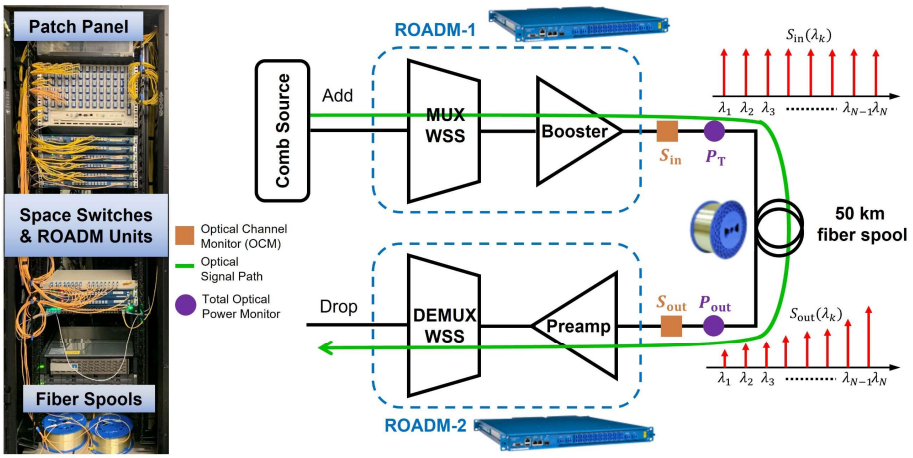

Fig. 1. (Left) The programmable optical network in the COSMOS testbed. (Right) Block diagram of the experimental set-up in COSMOS.

access COSMOS (Cloud-enhanced Open Software-defined MObile wireless testbed for city-Scale deployment) testbed [16]. The performance of this DNN model is then benchmarked against that of established analytical models in [12 – 14] to assess its accuracy and potential for applications in digital twins.

II. Methodology

In this section, we elucidate the experimental set-up in the COSMOS testbed which has been used for data collection, and then describe the channel loading configurations used therein.

A. Experimental Set-up

We conduct a series of experiments to collect extensive fiber measurements using the COSMOS testbed, deployed in Manhattan, New York City [16]. This state-of-the-art testbed is equipped with eight Lumentum graybox units, which can be interconnected through a variety of fiber spool lengths [16, 17]. The experimental setup within the COSMOS testbed is depicted in Fig. 1. It involves the use of two reconfigurable optical add-drop multiplexer (ROADM) units in conjunction with a single fiber spool. To emulate a WDM spectrum within the C-band, a comb source is employed to generate a total of 90 channels, each spaced at 50 GHz. These channels cover a spectrum ranging from $\lambda_1 = 1{,}529.16$ nm (196.05 THz) to $\lambda_{90} = 1{,}564.68$ nm (191.60 THz). The output from the comb source is directed to the add port of the MUX wavelength selective switch (WSS) in ROADM-1, which activates specific channels based on the channel loading configurations (described in Section II.B) by providing a very high attenuation to other channel wavelengths. Besides channel selection, ROADM-1 also ensures that the channel powers are flattened at the booster output (line-out) [3]. The power of each channel is adjusted to maintain an average power level of P_0, with a stringent condition that the deviation from the mean value is ≤ 0.2 dB. Once the WDM signal is appropriately configured, it is transmitted through a 50 km fiber spool. This signal is subsequently received at the pre-amplifier input (line-in) of the second ROADM unit (ROADM-2). At this point, the signal undergoes further processing and is eventually dropped after passing through the DEMUX WSS, which ensures that the relevant channels are accurately isolated and analysed.

To characterize the optical fiber under test, we perform two calibration tests before our main experiments. Firstly, we conduct a low calibration test by setting the input channel power to a very small value. This suppresses the non-linear effects in the fiber. Specifically, over each channel wavelength, a power of $P_0 = -20$ dBm is launched into the fiber. This test is essential for determining the wavelength-dependent linear loss of the fiber, which is calculated by analyzing the difference between the spectra $S_{out}(\lambda)$ and $S_{in}(\lambda)$ obtained during this test at the output and the input of the fiber, respectively. Secondly, we perform a high calibration test in which all 90 channels are fully loaded into the input spectrum, i.e., the launch power of each channel is set to a large value of $P_0 = 3.5$ dBm. The resulting output spectrum from this test is then used to calculate the normalized Raman gain coefficient γ, which is a key parameter in understanding the extent of Raman scattering and its influence on the overall system performance. These calibration experiments are crucial for establishing a baseline understanding of the fiber's performance characteristics.

For the primary experiments aimed at investigating the Raman effect, we systematically vary the number of channels loaded at the input of the fiber, testing a range of channel counts, $N \in \{2, 5, 10, 20, \ldots, 80, 90\}$. This approach allows us to observe how the distribution of channels influences the Raman tilt, providing valuable insights into the nonlinear dynamics at play within high-capacity optical transmission systems. To explore the phenomenon of Raman tilt in greater depth, we set the launch power of each channel to $P_0 = 3.5$ dBm. This higher power level is chosen to maximize the visibility of the Raman effect within the system, allowing for a more detailed study of its impact on signal transmission. We record the input and output spectra, $S_{\text{in}}(\lambda)$ and $S_{\text{out}}(\lambda)$, respectively, under various test conditions which are then used to obtain the Raman tilt as explained in Section III. Note that the measurement error for Raman tilt is $\pm$ 0.028 dB.

B. Channel Loading Configurations

When the input spectrum is not fully loaded, i.e., $N < 90$, the channels can be distributed in different configurations. In the present work, we consider four such scenarios as

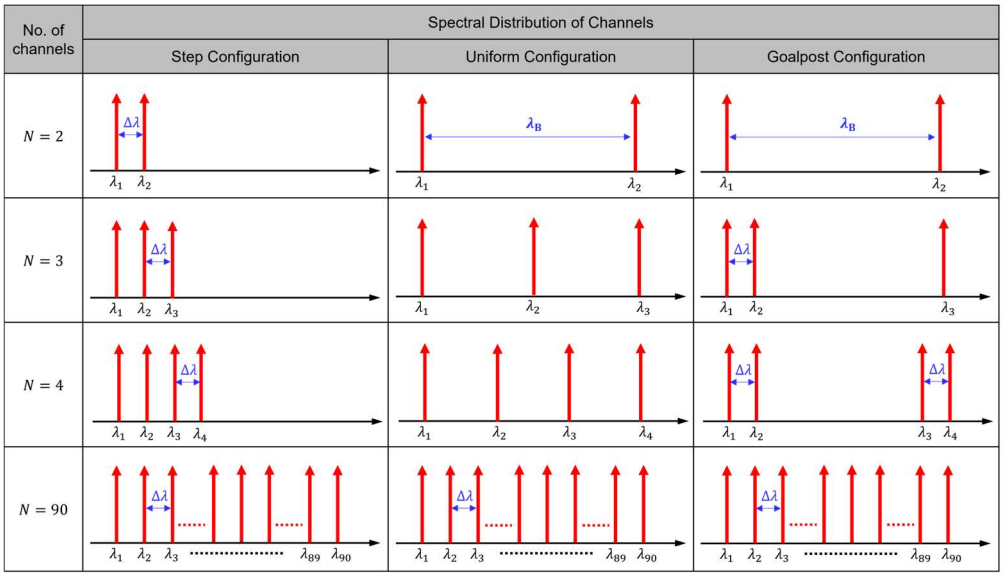

Fig. 2. Spectral distribution of channels in various channel loading configurations for different values of N. Here, $\Delta\lambda$ is the channel spacing and λ_B is the spectral bandwidth.

described below:

1) Step Configuration

Here, the channels are loaded from one end of the spectrum (starting with the lowest wavelength) at a fixed channel spacing of 50 GHz. However, as illustrated in Fig. 2, the total spectral bandwidth depends on N and increases as more channels are loaded.

2) Uniform Configuration

In this type of channel loading, the channels are distributed uniformly across the spectrum such that the total spectral bandwidth is fixed (refer Fig. 2). Consequently, when the number of channels is increased, the channel spacing reduces and the channels become more closely packed. Nevertheless, for a given value of N, the spacing between any two adjacent channels is always equal.

3) Goalpost Configuration

This is a type of bimodal configuration where channels are loaded from both ends of the spectrum such that there are two distinct bands, each containing equally spaced channels, as depicted in Fig. 2. As N is increased, the two bands gradually merge but the total spectral bandwidth remains fixed.

4) Random Configuration

The three scenarios elucidated above comprise systematic loading of channels. However, in practice, the channels are randomly distributed across the complete spectral band. For $N < 90$, the channels can occupy any N out of 90 possible spectral locations. Hence, for each value of N, there are ${}^{90}C_N$ different conceivable channel distributions, where ${}^{m}C_n$ is the binomial coefficient defined as ${}^{m}C_n = m!/n!\,(m-n)!$. Here, the channel spacing is, in general, uneven although the minimum channel spacing is bounded at 50 GHz. Moreover, the total spectral bandwidth is fixed. In the experimental set-up for random configuration, we generate 100 unique channel distributions for each value of N, and record the observations for all of them. Note that for $N = 90$, all four configurations have the same spectral distribution of channels.

III. Raman Tilt: Effects and Prediction

In this section, we briefly describe the Raman tilt and then discuss the analytical models for Raman tilt prediction. In a WDM system, Raman tilt occurs as a result of SRS which is a nonlinear optical phenomenon where optical power from higher frequency (shorter wavelength) channels is scattered into lower frequency (longer wavelength) channels as light propagates through the optical fiber. This energy transfer causes an asymmetric power distribution across the WDM spectrum, resulting in a spectral tilt, called Raman tilt, where the channel powers increase progressively from the shorter to the longer wavelengths. This tilt depends on the total power of the aggregate signals, and the distribution of that power across the spectrum (i.e., the wavelength locations of the signals) [13] and is modified by the wavelength-dependent (linear) fibre loss.

The tilt effect causes signal distortion, leading to signal degradation and performance issues in WDM systems. In particular, the spectral efficiency is degraded due to unequal channel power distribution which limits the effective use of available bandwidth. Moreover, the signal-to-noise ratio (SNR) across channels is imbalanced, leading to variations in service quality. Additionally, channels at lower wavelengths (with gain depletion) experience increased bit error rate (BER), necessitating more complex error correction and reducing overall data throughput. Furthermore, the energy efficiency is diminished due to higher pump power requirements which also exacerbate other nonlinear effects. As such, the prediction of Raman tilt in WDM systems is a critical part of managing optical networks, particularly as data rates increase and channels become denser.

Analytical prediction of Raman tilt in WDM systems involves using mathematical models that describe the nonlinear interactions within the fiber. These models provide the power levels of individual channels across the WDM spectrum which are then compared to obtain the Raman tilt. Consider a WDM system with N channels at wavelengths

$\lambda_k (k = 1, \dots, N)$. The time-independent power evolution along the fiber in this N-channel WDM system is denoted as

$$S(z,\lambda) = \sum_{k=1}^{N} p(z,\lambda_k)\delta(\lambda - \lambda_k) \quad (1)$$

where $p(z,\lambda_k)$ is the power carried by the channel wavelength λ_k at a distance z from the fiber input, such that $z = 0$ and $z = L$ correspond to the input and output of the fiber, respectively. Here, L is the total length of the optical fiber, and $\delta(.)$ is the Dirac delta function or unit impulse function. For discrete wavelengths in a WDM system, we can write $\delta(n) = 1$, for $n = 0$, else $\delta(n) = 0$. Neglecting other non-linearities like cross- and self-phase modulation, four-wave mixing, and non-linear polarization; the power exchange during SRS is denoted as [14]

$$\frac{d}{dz}p(z,\lambda_k) = -\alpha p(z,\lambda_k) + \sum_{j=1}^{N} g_{jk} p(z,\lambda_j) p(z,\lambda_k) \quad (2)$$

where α is the attenuation coefficient of the fiber and g_{jk} is the Raman gain coefficient between two channels with wavelengths λ_j and λ_k. Here, we also assume that no energy is lost when a short wavelength photon transforms into a longer wavelength photon due to SRS. The Raman tilt is then defined as the ratio of the output powers carried by the longest and shortest channel wavelengths at the fiber output.

$$\mathcal{R} = \frac{p(L,\lambda_N)}{p(L,\lambda_1)} \quad (3)$$

It is challenging to obtain the exact solutions of (2); ergo some simplified models have been proposed based on approximations and assumptions, as presented below.

1) Case I: Triangular Gain Approximation

Assuming that the Raman frequency shift is more than the total WDM bandwidth, the Raman gain coefficient is approximated to have a triangular profile expressed as $g_{jk} = 2\gamma A_{\text{eff}}(\lambda_k - \lambda_j)$ where A_{eff} is the effective core area of the fiber, and γ is a normalization constant [12]. This means that the Raman gain is assumed to vary linearly with frequency differences. Subsequently, in this case, the power of channel wavelength λ_k at the fiber output is given as [12]

$$p(z,\lambda_k) = \frac{p(0,\lambda_k) P_{\text{T}} \exp(-\alpha z)}{\sum_{j=1}^{N} p(0,\lambda_j) \exp\{\gamma P_{\text{T}} L_{\text{eff}}(\lambda_j - \lambda_k)\}} \quad (4)$$

where $p(0,\lambda_k)$ is the input power carried by the channel wavelength λ_k and $P_{\text{T}} = \sum_{k=1}^{N} p(0,\lambda_k)$ is the total power input to the fiber. Moreover, $L_{\text{eff}} = (1 - \exp(-\alpha L))/\alpha$ is the effective length of the fiber.

2) Case II: Rectangular Spectrum Assumption

In addition to the approximation in Case I, it is further assumed that the spectrum of the WDM signal is rectangular in shape. In other words, all channels have the same input power, i.e., $p(0,\lambda_k) = P_0 \; \forall \, k \in \{1, 2, \dots, N\}$. Imposing this on (4), we get the fiber output power in this case as

$$p(z,\lambda_k) = \frac{P_{\text{T}} \exp(-\alpha z)}{\sum_{j=1}^{N} \exp\{\gamma P_{\text{T}} L_{\text{eff}}(\lambda_j - \lambda_k)\}} \quad (5)$$

Note that this simplification assumes a strictly flat input spectrum.

3) Case III: Equally Spaced Channels Assumption

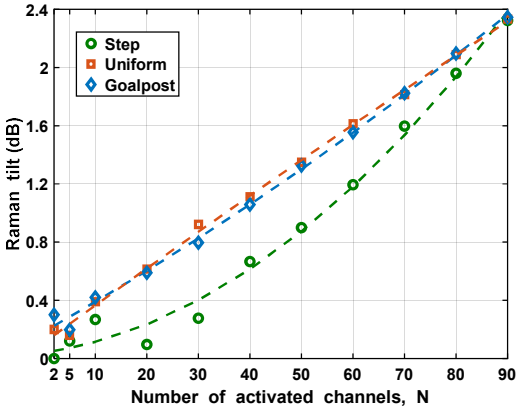

Fig. 3. Raman tilt obtained from experimental observations for different channel loading configurations. The dotted lines are fitted curves.

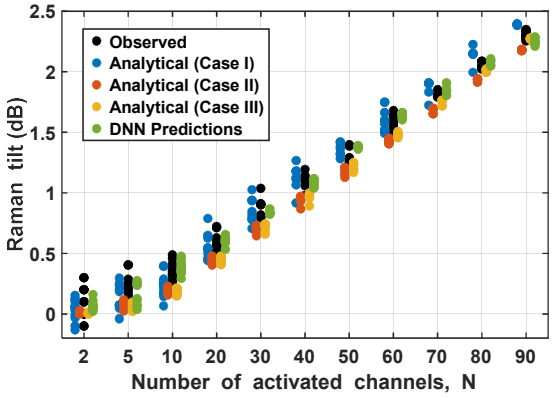

Fig. 4. Raman tilt for random channel loading configuration obtained using experimental observations, various analytical prediction methods and the proposed DNN prediction model.

In this case, the model is further simplified by assuming that the spacing between any two adjacent channels is equal, such that any channel λ_j can be expressed in terms of the first channel wavelength λ_1 as $\lambda_j = \lambda_1 + (j-1)\Delta\lambda$ where $\Delta\lambda$ is the separation between two adjacent channel wavelengths. Hence, in this case, the power at the fiber output is

$$p(z,\lambda_k) = \frac{P_{\text{T}} \exp(-\alpha z)}{\sum_{j=1}^{N} \exp\{\gamma P_{\text{T}} L_{\text{eff}}(j-k)\Delta\lambda\}} \quad (6)$$

This model has been used in [13] where authors study the uniform channel loading configuration as described in Section II.B. Having obtained the powers of the first ($k = 1$) and last ($k = N$) wavelengths at the fiber output ($z = L$) using Eqns. (4), (5) and (6), we can predict the Raman tilts for the three models in Cases I, II, and III, respectively.

IV. Results and Discussion

In this section, we present the results obtained in our work using the experimental methodology and prediction models detailed in Sections II and III, respectively. We also introduce the proposed DNN model for Raman tilt prediction and evaluate its performance for use in digital modelling.

A. Experimental Results

We report values of Raman tilt determined using the data obtained from experiments described in Section II.A. In Fig. 3, we depict the variation in Raman tilt with an increasing number of activated channels, N for three different channel loading configurations, viz. step, uniform and goalpost (refer Section II.A). A quadratic curve fitting is performed on the

experimental values, shown as dotted lines in Fig. 3. We observe that the Raman tilt is aggravated as N is increased because addition of more channels augments the Raman effect. Moreover, the Raman tilt values for uniform and goalpost configurations are similar, and these are higher than those for step configuration. This is due to the smaller channel spacings in the latter case. Specifically, the Raman tilt increases from ~0.2 dB at $N = 2$ to ~2.4 dB at $N = 90$, for uniform and goalpost configurations, whereas it varies from ~0 dB at $N = 2$ to ~2.4 dB at $N = 90$ for the step configuration. Evidently, for $N = 90$, all values overlap because the input spectra are the same for all three configurations (refer Fig. 2). However, these systematic channel loading configurations do not emulate practical scenarios where the channel loading is random. Therefore, we focus on the random channel configuration (refer Section II.A) and obtain the Raman tilt for this case. Similar to other configurations, the random configuration also exhibits an increasing trend in Raman tilt when more channels are activated.

B. Analytical Prediction of Raman Tilt

We now employ the analytical models described in Section III to predict the Raman tilt with different channel configurations. In Fig. 4, we also plot the Raman tilt values predicted by the analytical models (Case-I, Case-II, and Case-III) for the random channel configuration. We do a similar analysis for step, uniform and goalpost channel loading configurations in Fig. 5, where we also depict the fitted curves obtained from experimental data. We deduce that, in all four configurations, the plots of the analytical predictions follow the same shapes and trends as the corresponding fitted curve for observed results. However, the predictions are considerably distinct from the actual values obtained from experimental observations, with a maximum deviation of ~0.3 dB. While Case-II and Case-III provide optimistic predictions of lower tilt values, Case-I presents a pessimistic estimate of higher tilt values.

TABLE I. DNN ARCHITECTURE

Input features	Total launch power, No. of channels, Channel distribution
Output features	Raman tilt values
Optimization algorithm	Adam optimizer
Activation function	Exponential linear unit (ELU)
No. of hidden layers and neurons	5 with 64/64/2/64/64 neurons
Loss function	Mean squared error (MSE)
Weight initilaisation	Kaiming normalization
Learning rate	0.01

C. DNN-based Model for Raman Tilt Prediction

We design a DNN-based model to predict the Raman tilt in optical fibers deployed in systems with arbitrarily loaded channels. Table I lists the structural details of the proposed DNN model. The dataset comprises observations recorded from experiments on the COSMOS testbed with all four channel loading configurations. The data from the random configuration is split in the ratio 8:1:1 for training, validation, and testing, respectively. The DNN model is trained for 100 epochs to ensure convergence. In Fig. 4, we present the

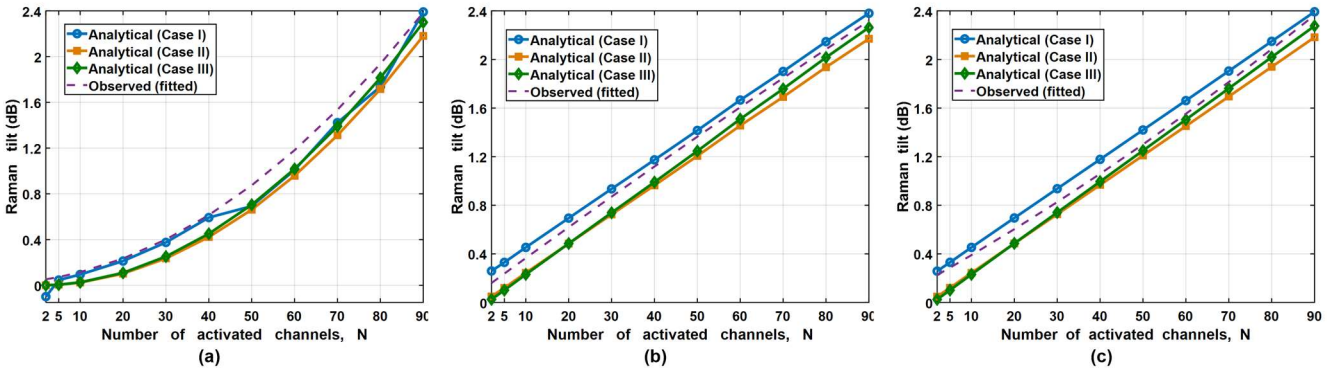

Fig. 5. Raman tilt obtained from experimental observations and predicted using different analytical models (Case-I, Case-II, Case-III) for channels loaded in (a) Step configuration, (b) Uniform configuration, and (c) Goalpost configuration.

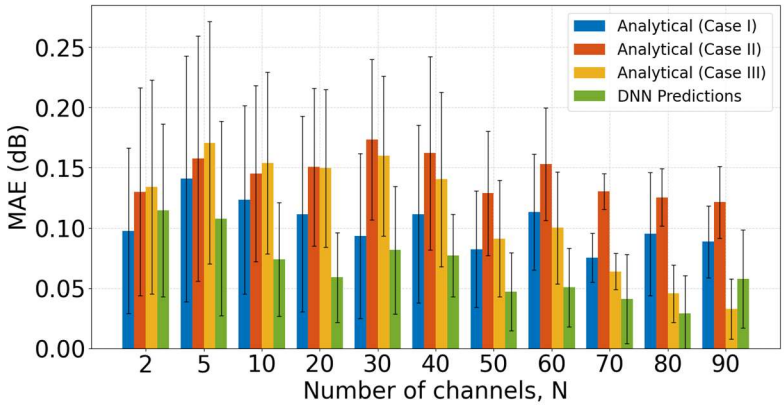

Fig. 6. Mean absolute error (MAE) values achieved by the analytical and DNN-based prediction models for the random channel configuration.

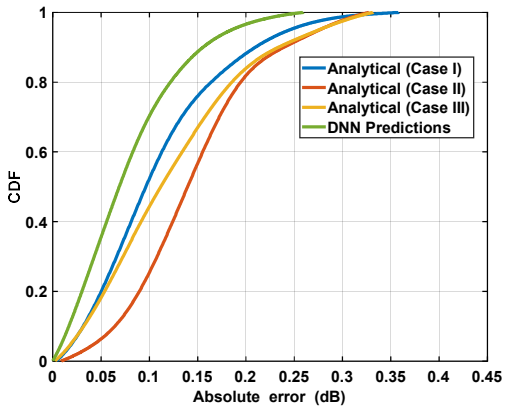

Fig. 7. CDFs of absolute errors achieved by the analytical and DNN-based prediction models for the random channel configuration.

Raman tilt values predicted by the proposed DNN model using the test set with random channel loading configuration. The analytical predictions are also generated using the same test set. We infer that the predictions not only have the same trend as the observed case, but they are also notably similar.

D. Performance Evaluation of the Proposed Digital Twin

We now evaluate the performance of the proposed DNN-based model in terms of its prediction error and compare its performance with those of the analytical models across varying numbers of channels in the random configuration. In Fig. 6, we present the mean absolute error (MAE) achieved by the DNN-based model and the analytical models described in Section III. Clearly, the DNN model achieves the lowest MAE among all prediction models with a minimum of 0.03 dB at $N = 80$. The DNN's performance is limited by the measurement error (± 0.028 dB) in data collection. We also plot the cumulative density functions (CDFs) of the absolute error values for all prediction models, as depicted in Fig. 7. For a quantitative comparison, in Table II, we list the performance metrics (maximum values, percentiles and medians) obtained from the CDFs of absolute errors. We infer that the DNN model has the best error performance. Among the analytical models, Case-I has superior performance which is expected as this case has the least number of assumptions.

V. Conclusion

We design a DNN model to predict the Raman tilt in ROADM-based transmission systems. For training, validation and testing of the proposed DNN model, we collect data through experiments involving WDM transmissions with various channel distributions in the COSMOS testbed. Additionally, we present a comprehensive analysis of the physics-based analytical models for Raman tilt prediction. We deduce that the Raman tilt varies from ~0 dB to ~2.4 dB under different channel loading scenarios. We also analyse the error performance of the prediction models to infer that the prediction errors are satisfactorily low ($\leq$ 0.3 dB). Evidently, the proposed DNN model achieves the lowest prediction error of 0.03 dB. Our results demonstrate the DNN's potential for enhancing the accuracy of digital twins in optical communication networks, offering a promising avenue for addressing the complex control challenges in next-generation networks. As a future extension of this work, it would be interesting to study the Raman tilt prediction in the presence of practical impairments like discrete fiber losses, amplifier ripple etc.

TABLE II. Comparison of Predcition Models based on CDFs of Absolute Errors

Prediction Model	Performance Metrics (in dB)				
	25th Percentile	Median	75th Percentile	90th Percentile	Max Value
Case-I	0.06	0.09	0.13	0.24	0.36
Case-II	0.10	0.14	0.18	0.28	0.33
Case-III	0.06	0.10	0.16	0.29	0.33
DNN	0.03	0.06	0.10	0.18	0.26

Acknowledgements

This work was supported in part by NSF grants CNS-1827923, OAC-2029295, CNS-2112562, and CNS-2330333; SFI under grants 13/RC/2077 P2 and 22/FFP-A/10598; and EU under MSCA Grant No. 101155602.

References

[1] A. Fayad, T. Cinkler and J. Rak, "Toward 6G optical fronthaul: A survey on enabling technologies and research perspectives," *IEEE Communications Surveys & Tutorials*, Jun. 2024 (Early Access).

[2] E. Akinrintoyo *et al.*, "Reconfigurable topology testbeds: A new approach to optical system experiments," *Optical Fiber Technology*, vol. 76, pp. 10324, 2023.

[3] Z. Wang, D. Kilper and T. Chen, "Open EDFA gain spectrum dataset and its applications in data-driven EDFA gain modeling," *Journal of Opt. Communications and Networking*, vol. 15, no. 9, pp. 588-99, 2023.

[4] F. Musumeci *et al.*, "An overview on application of machine learning techniques in optical networks," *IEEE Communications Surveys & Tutorials*, vol. 21, no. 2, pp. 1383-1408, 2019.

[5] A. Lord, "The future of optical transport: Architectures and technologies from an operator perspective," in *Proc. Optical Fiber Communication Conference*, San Diego, USA, 2022, pp. 1-18.

[6] M. Rodrigo *et al.*, "Digital twins for 5G networks: A modeling and deployment methodology," *IEEE Access*, vol. 11, pp. 38112-26, 2023.

[7] Y. Hui *et al.*, "Digital twins for intelligent space-air-ground integrated vehicular network: Challenges and solutions," *IEEE Internet of Things Magazine*, vol. 6, no. 3, pp. 70-76, 2023.

[8] S. Mihai *et al.*, "Digital twins: A survey on enabling technologies, challenges, trends and future prospects," *IEEE Communications Surveys & Tutorials*, vol. 24, no. 4, pp. 2255-2291, 2022.

[9] Z. Wang *et al.*, "Multi-span optical power spectrum prediction using ML-based EDFA models and cascaded learning," in *Proc. Optical Fiber Communication Conference*, San Diego, USA, 2024, pp. 1-3.

[10] A. Raj *et al.*, "Self-normalizing neural network, enabling one shot transfer learning for modeling EDFA wavelength dependent gain," in *Proc. European Conference on Optical Communications*, Glasgow, UK, 2023, pp. 748-751.

[11] C. Lasagni, P. Serena, A. Bononi and J. -C. Antona, "A generalized Raman scattering model for real-time SNR estimation of multi-band systems," *Journal of Lightwave Technology*, vol. 41, no. 11, pp. 3407-3416, Jun. 2023.

[12] M. Zirngibl, "Analytical model of Raman gain effects in massive wavelength division multiplexed transmission systems," *Electronics Letters*, vol. 34, no. 8, pp. 789-790, Apr. 1998.

[13] S. Bigo, S. Gauchard, A. Bertaina and J. -P. Hamaide, "Experimental investigation of stimulated Raman scattering limitation on WDM transmission over various types of fiber infrastructures," *IEEE Photonics Technology Letters*, vol. 11, no. 6, pp. 671-673, Jun. 1999.

[14] F. Vanholsbeeck *et al.*, "Raman-induced power tilt in arbitrarily large wavelength division multiplexed systems," *IEEE Photonics Technolo--gy Letters*, vol. 17, no. 1, pp. 88-90, Jan. 2005.

[15] R. Raj *et al.*, "Machine learning-based Raman tilt prediction in a ROADM transmission system," in *Proc. European Conference on Optical Communications*, Glasgow, UK, 2023, pp. 1504-1507.

[16] COSMOS Testbed Main Site [online] Available: https://www.cosmos-lab.org/ (accessed Aug. 10, 2024).

[17] T. Chen *et al.*, "A software-defined programmable testbed for beyond 5G optical-wireless experimentation at city-scale," *IEEE Network*, vol. 36, no. 2, pp. 90-99, 2022.